J. Fluid Mech. (1978), *vol.* 87, *part* 1, *pp.* 179–192
Printed in Great Britain

Flow over a containment dyke

By H. P. GREENSPAN
Mathematics Department, Massachusetts Institute of Technology, Cambridge
AND R. E. YOUNG
S. Ross & Co., Boston, Massachusetts 02110

(Received 13 September 1977)

The wall of a large tank or reservoir breaks, sending fluid against a secondary containment dyke. The impact of the surging fluid against the safety barrier is studied. The results of theoretical analysis and numerical simulation (for vertical dykes) are in good agreement with experimental data concerning overflow and total spillage as well as the fluid motion after collision, including the development and formation of a strong shock. The dependence of spillage on the inclination of the dyke is also determined by experiment.

1. Introduction

Safety regulations sometimes require that a tank storing a dangerous liquid be surrounded by an impounding dyke in order to contain any accidental spillage. For this purpose, the volume capacity of the dyke usually approximates that of the storage facility, which can be several million cubic feet.

We examine the consequences of a sudden, massive rupture or collapse of the tank wall which releases a large volume of liquid in a relatively short period of time. Dykes have not been designed to prevent the overflow of a rushing liquid and a substantial part of the stored fluid can surge over the impounding wall and escape from the containment area. Indeed, very little is actually known about fluid impact against and flow over a barrier, and these transient problems are studied here both theoretically and experimentally.

2. Formulation

The collapse of a large section of tank wall, as the result of, say, an earthquake or accident, releases a mound of liquid which moves rapidly and impacts upon the containment dyke. The fluid surmounts the barrier and the manner in which this happens depends in part on the shape of the dyke. The rushing liquid may simply vault an inclined side, or it may pile up very rapidly at the face of a vertical wall and then flow over the top. In either case, a strong shock wave forms at the dyke and returns towards the storage tank. Clearly, the process is a very complicated and highly nonlinear dynamical interaction. However, the essential features of the surge and overflow can be elucidated by examining the fluid motion in the simplest and most ideal conditions. To this end, we consider the two-dimensional configuration shown in figure 1 (which when revolved about the vertical axis at $x = -R$ generates the more

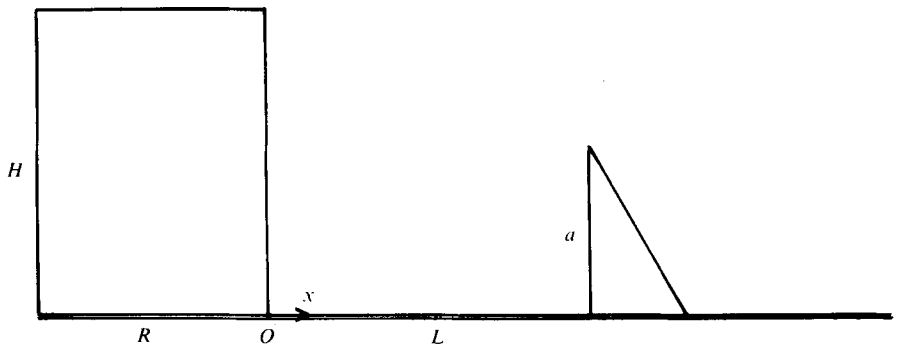

FIGURE 1. Defining diagram and cross-section of a storage tank in a finite reservoir and a containment dyke. The removable wall is at the origin.

typical geometry of a cylindrical storage tank surrounded by a circular dyke). Liquid is released when the wall of the tank at $x = 0$ is removed at time zero; the flow is then directed against a dyke of height a placed at $x = L$. The impact surface of the barrier is taken to be vertical in the theoretical analysis; flow over an inclined dyke is examined here only by experiment.

In the experimental arrangement, the tank is a 9 in. cube one wall of which is a movable slide that is pulled out quickly to simulate a massive rupture. The water flows into a long channel that is open at the other end. Figure 2 (plate 1) is a typical sequence of photographs showing the fluid motion after release. (The total time period pictured is about 1 s.) Water rushing towards the dyke at high speed catapults high into the air upon collision. The fluid piles up and pours over the dyke as a bore returns to the region of collapse.

The overflow, designated by Q_0 and defined as the fraction of the original fluid volume that escapes upon impact, is the primary quantity of interest and importance. The object of theory is a correct qualitative and quantitative description of events, meaning that the spillage can be calculated and its dependence on the various parameters ascertained. This may be accomplished by employing the nonlinear shallow-water theory, which has been applied with remarkable success in 'dam-break' problems of the type under investigation.

The nonlinear shallow-water equations are in essence depth-averaged versions of the conservation laws of mass and momentum in which the dependent variables are the free-surface height $h(x,t)$ and the mean horizontal velocity $u(x,t)$:

$$[(h-h_G)u]_x = -h_t, \tag{2.1}$$

$$u_t + uu_x = -gh_x. \tag{2.2}$$

The quantity

$$c = [g(h-h_G)]^{\frac{1}{2}}, \tag{2.3}$$

which is the wave speed of a disturbance in the flow, plays a fundamental role in the theory. Here g is the acceleration due to gravity and $h_G(x)$ is the elevation of the dry ground above some reference level; $h-h_G$ then measures the depth of the fluid.

It is assumed that the terrain between the tank and the vertical dyke is level and smooth, so that $h_G = 0$ (but in more complicated geometries, including inclined-dyke problems, topographic variations are important and must be included). Viscosity,

turbulence and ground resistance have been neglected. The errors introduced by these approximations are found to be acceptable, although the theory can be modified to account for such effects (Dressler 1954; Whitham 1955).

Equations (2.1) and (2.2) can be rewritten as

$$2(c_t + uc_x) + cu_x = 0, \tag{2.4}$$

$$u_t + uu_x + 2cc_x = 0. \tag{2.5}$$

The specification of initial and boundary conditions completes the formulation of the problem. For $t \leqslant 0$, the quiescent fluid fills the tank, so that

$$u(x, 0) = 0, \quad c(x, 0) = (gH)^{\frac{1}{2}} \quad \text{for} \quad -R \leqslant x \leqslant 0. \tag{2.6}$$

The wall of the tank at $x = 0$ is then removed instantaneously and the water rushes over a dry bed towards the vertical dyke at $x = x_w = L$. After impact, the fluid velocity at the dyke is zero until the water level there exceeds the height a of the barrier and overflow begins. With $c_0^2 = ga$, this can be expressed as

$$u(x_w, t) = 0 \quad \text{for} \quad c(x_w, t) \leqslant c_0.$$

An appropriate condition is required to describe overflow.

If the height h_w of the fluid at the impounding wall is larger than a then the water level on top of the dyke at $x = x_w$ is $h_w - a$, and the local wave speed there is

$$\tilde{c} = [g(h_w - a)]^{\frac{1}{2}}.$$

We assume that fluid which passes over the barrier ceases to influence the main body of water still within the containment area. This is assured by setting $\tilde{u} = \tilde{c}$, where $\tilde{u}$ is the fluid velocity upon the dyke. (The convected propagation velocities are then positive and no 'signal' can travel backwards.) Since the conservation of mass requires $u_w h_w = \tilde{u}(h_w - a)$, these relationships can be combined as

$$u = (c^2 - c_0^2)^{\frac{1}{2}} c^{-2} H(c - c_0) \quad \text{at} \quad x = x_w, \tag{2.7}$$

where the Heaviside function

$$H(x) = \begin{cases} 1, & x > 0, \\ 0, & x < 0, \end{cases}$$

is used to incorporate different conditions at this boundary into one succinct formula.

The condition at the other, intact wall of the tank is

$$u = 0 \quad \text{at} \quad x = -R. \tag{2.8}$$

The height of the tank H and the time $(H/g)^{\frac{1}{2}}$ are characteristic scales that are used to make the problem dimensionless by the following transformations:

$$x \to Hx, \quad t \to (H/g)^{\frac{1}{2}} t, \quad h \to Hh, \quad u \to u(gH)^{\frac{1}{2}}, \quad c \to (gH)^{\frac{1}{2}}.$$

The basic equations (2.4) and (2.5) remain unchanged in this non-dimensionalization, as does the overflow condition (2.7). Equation (2.6) is now

$$u(x, 0) = 0, \quad c(x, 0) = 1 \quad \text{for} \quad -R/H \leqslant x \leqslant 0 \tag{2.6a}$$

and (2.8) holds at $x = -R/H$.

Since the motion obviously involves the development and propagation of a shock as well as the reverberation and interaction of all wave disturbances, the following shock conditions are required in the analysis.

Let subscripts f and b denote the front and back of the shock, i.e. the regions into and from which the shock moves in the next instant of time. If U is the shock velocity and $M = c_b/c_f$, then the forms of the jump conditions that will be most convenient to use are

$$\left.\begin{aligned} U &= u_f - \frac{c_f}{2^{\frac{1}{2}}} M^2 \left(1+\frac{1}{M^2}\right)^{\frac{1}{2}}, \\ u_b &= u_f - \frac{c_f}{2^{\frac{1}{2}}} (M^2-1)\left(1+\frac{1}{M^2}\right)^{\frac{1}{2}}. \end{aligned}\right\} \tag{2.9}$$

We turn now to the solution of the problem.

3. Theoretical analysis

The propagation and reflexions of the shock and the principal rays divide the x, t space $-R/H \leqslant x \leqslant L/H$, $t \geqslant 0$ into the distinct regions illustrated in figure 3. It is then convenient to describe the solution in each domain, as well as the particular analytical and/or numerical methods employed.

After the wall of the tank at $x = 0$ has been removed, water rushes towards the dyke at $x = x_w = L/H$, and a rarefaction wave moves into the tank. During this early stage, the fluid in region I is still at rest whereas region II is devoid of water. The solution of the equations of motion in region III, which is identical to that for the classical dam-break problem, is

$$u = \tfrac{2}{3}(1+x/t), \quad c = \tfrac{1}{3}(2-x/t). \tag{3.1}$$

The leading edge of the fluid, which corresponds to $c = 0$, moves with the constant dimensionless speed 2 [i.e. twice the natural propagation speed $(gH)^{\frac{1}{2}}$] and reaches the dyke at time $t_w = \frac{1}{2}x_w$. Meanwhile, a rarefaction wave propagates at a constant velocity of unity in the reverse direction and reflects off the rear wall at $x = -R/H$ when $t = R/H$.

Upon collision of the fluid with the vertical face of the dyke, water accumulates rapidly and to a great height; a strong shock forms and moves, slowly at first, back towards the tank. Since the edge of the advancing fluid front has zero thickness in the inviscid theory, impact must be examined analytically, and with care, in order to provide the data to initialize a numerical program. Therefore let the shock locus be described by $x_s(t)$ for $t \geqslant t_w$ with $x_s(t_w) = x_w$ and $x_s'(t) < 0$. For some time after impact, the flow into which the shock is advancing is given by (3.1). A solution of the basic equations is then sought in domain V between the shock and the dyke, $x_s \leqslant x \leqslant x_w$, which satisfies the shock conditions given in (2.9) and the overflow condition (2.7).

The study of impact is facilitated by introducing space and time variables centred at the point of collision as follows:

$$\eta = (x_w - x)/t_w, \quad \tau = (t-t_w)/t_w, \quad \text{where} \quad x_w = 2t_w. \tag{3.2}$$

Furthermore, we define

$$\zeta = \eta/\tau^2 \tag{3.3}$$

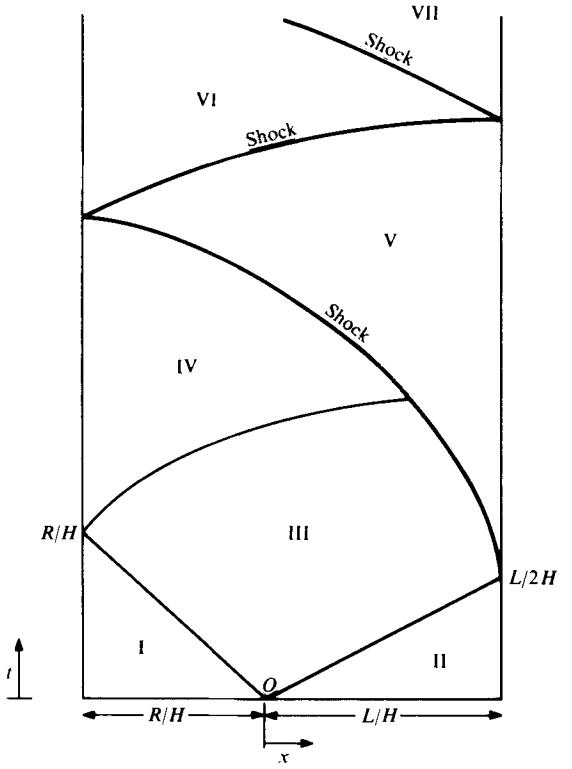

FIGURE 3. Regions of x, t space delineated by the loci of the shock and the principal rays.

and represent all the flow variables as power series in τ in the region between the shock, $\zeta_s = \eta_s/\tau^2$, and the barrier, $\zeta = 0$:

$$\left.\begin{aligned} u &= \tau f_0(\zeta) + \tau^2 f_1(\zeta) + \ldots, \\ c &= \tau^{\frac{1}{2}}[g_0(\zeta) + \tau g_1(\zeta) + \ldots]. \end{aligned}\right\} \tag{3.4}$$

The shock locus is written as $\zeta_s = z(\tau) = z_0 + z_1\tau + \ldots$ (3.5)

and the shock velocity by implication is

$$U = -d\eta_s/d\tau = -d[\tau^2 z(\tau)]/d\tau = -(2z_0\tau + 3z_1\tau^2 + \ldots). \tag{3.6}$$

The substitution of these series into the equations of motion (2.4) and (2.5), the conditions (2.9) at the shock and the conditions (2.7) (before overflow) at the wall yields

$$\left.\begin{aligned} f_0(\zeta) &= \zeta, \quad f_1 = \frac{5}{3}\frac{\zeta^3}{k_0^2} + \frac{2k_1\zeta}{k_0}, \\ g_0(\zeta) &= k_0, \quad g_1 = -\frac{\zeta^2}{2k_0} + k_1, \\ z_0 &= \frac{8}{27k_0^2}, \quad z_1 = -\frac{1}{4}\left[f_1(z_0) + \frac{6z_0}{k_0}g_1(z_0) + 8z_0 - 6z_0^2\right], \end{aligned}\right\} \tag{3.7}$$

where $$k_0 = 2^{\frac{1}{4}}3^{-\frac{1}{2}}, \quad k_1 = -\frac{5}{9}\frac{3^{\frac{1}{2}}}{2^{\frac{1}{4}}}(2^{\frac{1}{2}} - \tfrac{1}{6}).$$

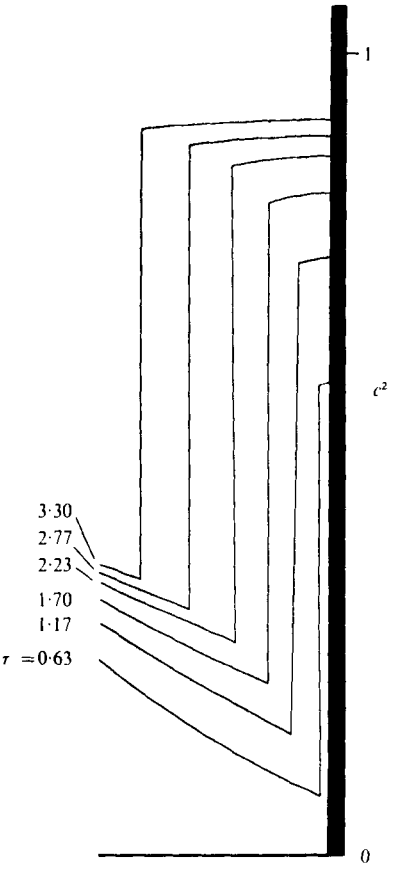

FIGURE 4. Water level c^2 near the dyke and across the shock for several values of the scaled time following impact.

The numerical values of the constants are

$$k_0 = 1{\cdot}373178, \quad k_1 = -1{\cdot}054409, \quad z_0 = 0{\cdot}157135, \quad z_1 = -0{\cdot}035232,$$
$$g_1(z_0) = -1{\cdot}063400 \quad \text{and} \quad f_1(z_0) = -0{\cdot}237886.$$

Equations (3.4)–(3.7) give the entire solution in region V for a short period following impact. At this time, water is rapidly piling up at the dyke behind the shock. Soon fluid will begin to flow over the barrier and/or the reflected waves will interact with the propagating shock (the boundary between IV and V). In either case the series solution then ceases to be valid. Examination of the formulae for $x_s(t)$ and c^2 shows that water accumulates quickly at the dyke because the shock is very slow in starting. Moreover, the free-surface height behind the bore is nearly uniform at any instant of time (figure 4). This is the basis of an analytical approximation which enables the motion in V to be determined for much longer times when the wall of the dyke is too high to allow any overflow.

An integral form of the conservation of mass states that all the water that passes through the shock accumulates beyond the shock if the wall is 'infinitely' high:

$$\int_{x_s}^{2t} c_{\mathrm{III}}^2 \, dx = \int_{x_s}^{2t_w} c_{\mathrm{V}}^2 \, dx, \tag{3.8}$$

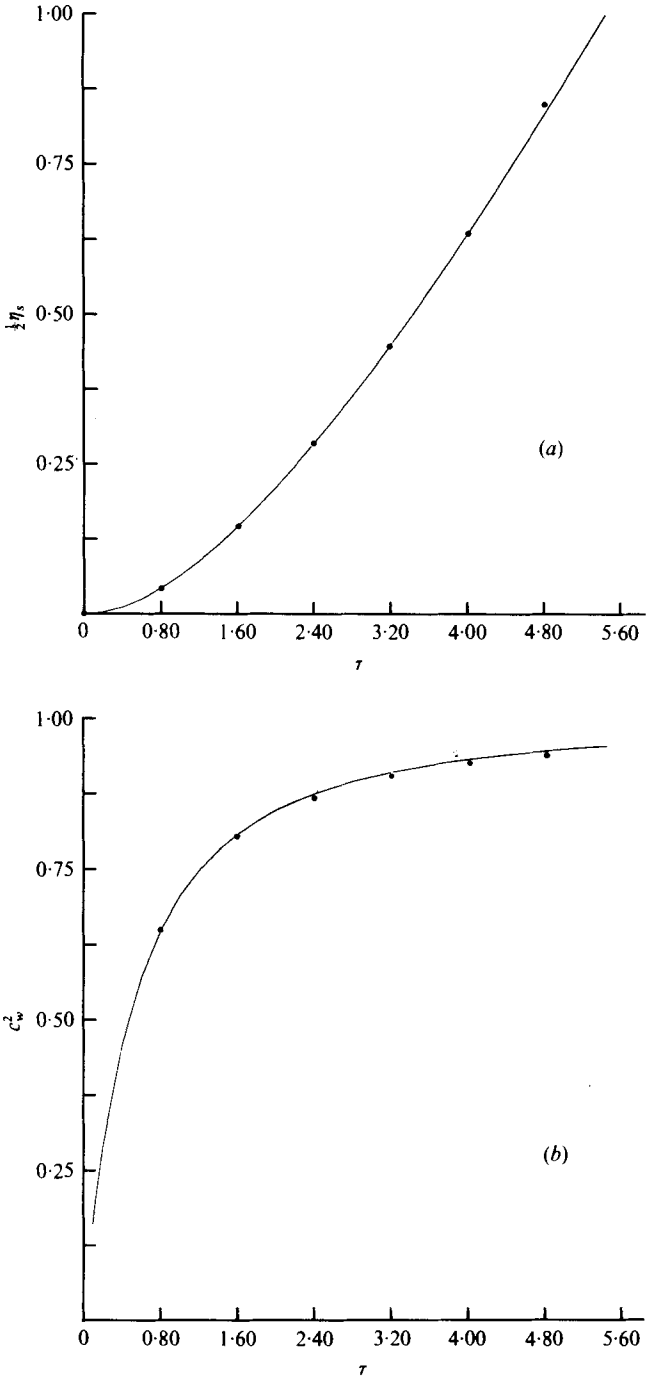

FIGURE 5. (*a*) Shock position *vs.* time following impact. (*b*) Water level at the dyke. ——, numerical calculation; ●, analytical approximation, equations (3.9) and (3.10).

where c_{III} and c_{V} are the propagation speeds in the designated regions. In particular, $c_{\mathrm{III}}^2 = \frac{1}{9}(2 - x/t)^2$. If c_{V}^2 is approximated as a function of time only, then the substitution of this formula in (3.8) yields

$$c_{\mathrm{V}}^2 \simeq \frac{t(2 - x_s/t)^3}{27(2t_w - x_s)}. \tag{3.9}$$

Now condition (2.9) on the shock velocity (with the identifications $c_f = c_{\mathrm{III}}$, $u_f = u_{\mathrm{III}}$, $c_b = c_{\mathrm{V}}$) is used to obtain a differential equation for $x_s(t)$ or equivalently for $\eta_s(\tau)$:

$$\frac{d\eta_s}{d\tau} = -\frac{2}{3}\left(\frac{3 + \tau - \eta_s}{1 + \tau}\right) + \frac{1}{3 \times 2^{\frac{1}{2}}}\left(\frac{2\tau + \eta_s}{1 + \tau}\right) M^2 \left(1 + \frac{1}{M^2}\right)^{\frac{1}{2}}, \tag{3.10}$$

where

$$M^2 = (2\tau + \eta_s)/3\eta_s. \tag{3.11}$$

For small values of τ,

$$\eta_s = \tfrac{1}{9} \times 2^{\frac{1}{2}}\tau^2 - \tfrac{1}{54}(2^{\frac{3}{2}} - 1)\,\tau^3 + \ldots. \tag{3.12}$$

The comparison of this approximate formula with the exact result given in (3.5) shows only a slight difference in the respective coefficients of τ^3 ($-0{\cdot}03386$ *vs.* the exact value $-0{\cdot}03523$). Equation (3.10) is integrated forwards in time using (3.12) or preferably (3.5) to specify the variables at the early time $\Delta\tau$. The results for the shock locus and the water level at the dyke are shown in figure 5.

Integral approximations of the mass and momentum conservation laws in the region behind the shock can also be adapted to study overflow. This extension of the theory is not presented because at best the results duplicate those obtained from the efficient numerical solution of the complete problem in regions V, VI and beyond. Unfortunately, the complicated wave interactions in these domains do necessitate use of the computer.

4. Numerical analysis

The numerical computations are based on the characteristic form of the equations of motion:

$$u \pm 2c = \text{constant on } dx/dt = u \pm c \quad (C_{\pm} \text{ characteristics}). \tag{4.1}$$

The computer program is used primarily to determine the flow in the later and more complicated situations in regions IV, V and beyond. (However, the numerical methods are checked in detail by their ability to reproduce accurately the exact theoretical solution in regions I, II and III.) The analysis of the initial impact of the surge against the dyke and the formation and propagation of the shock provides the data, (3.4)–(3.7), that are required to start the computer routine.

The calculations at time t proceed from the known values of u and c at an earlier time and at the physical boundaries $x = -R/H$ and $x = L/H$. The dependent variables are represented by values at a grid along the x axis, using linear interpolation to define points between nodes. The physical positions of these nodal points differ at successive times in order that the shock always lies between two nodes, at which points the values of the dependent variables satisfy the shock conditions. The nodes within each region are uniformly spaced; their number depends on the relative lengths of the regions separated by the shock and on the total number of nodes allocated. Calculations are advanced in time by the method of characteristics, equations (4.1). Thus, to determine

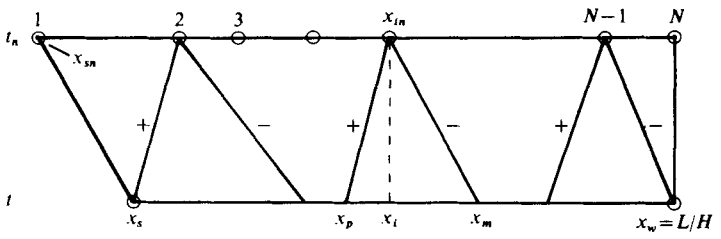

(*a*)

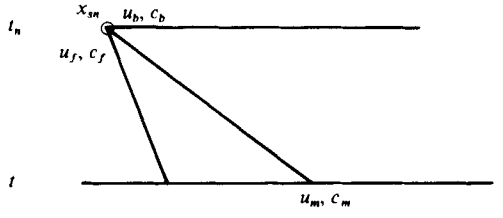

(*b*)

FIGURE 6. Defining diagrams for numerical grids.

u_{in} and c_{in} at the position x_{in} and at the new time t_n (see figure 6*a*) the following algorithm is applied:

(i) Calculate u_i and c_i at the same x position x_i, but at the old time t.

(ii) Determine x_p, the x position at the old time whose plus-characteristic passes through x_{in}:

$$(x_{in}-x_p)/(t_n-t) = u_i+c_i. \tag{4.2}$$

(iii) Obtain u_p and c_p at x_p.

(iv) Similarly, evaluate x_m using the minus-characteristic, u_i and c_i, then interpolate to find u_m and c_m.

(v) Calculate u_{in} and c_{in} from the simultaneous equations

$$u_p + 2c_p = u_{in} + 2c_{in} \tag{4.3}$$

and

$$u_m - 2c_m = u_{in} - 2c_{in}. \tag{4.4}$$

(vi) Use these results as starting conditions for determining u_{in} and c_{in} from central-difference formulae.

(vii) Recalculate x_p and x_m from the average of u and c at the old and new time end points of the characteristics obtained in the previous iteration.

(viii) Redetermine u_p, c_p, u_m, c_m, u_{in} and c_{in} and continue the process until the successive x_p's and x_m's differ insignificantly from previous values.

At the dyke $x = x_w$, we require that $t_n - t$ be sufficiently small that all interior nodes at t_n lie between the plus-characteristic through the shock position at t and the minus-characteristic through x_w. In this way, problems of interpolating along the wall or the shock are avoided. Linear interpolations are employed using data defined at node

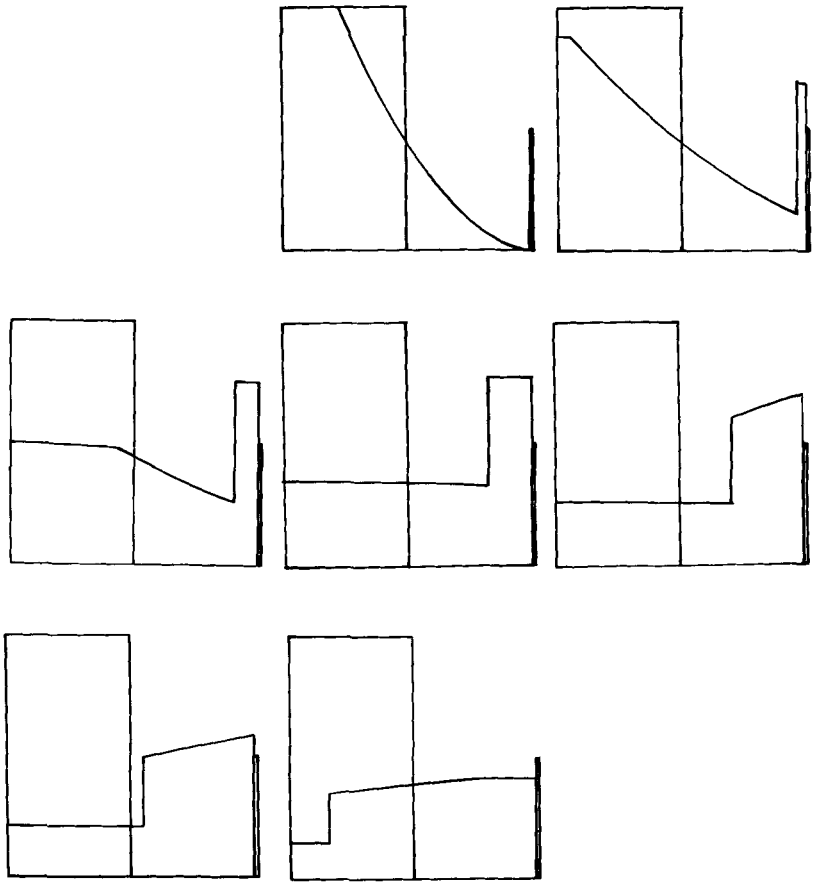

FIGURE 7. Computer simulation of the collapse and surge shown in figure 2. The graphs are arranged in correspondence with the photo sequence.

points along the segment between x_s and x_w to determine u and c at points not coinciding with nodal values from the two adjacent nodes.

At the shock, the jump conditions (2.9) are invoked along with the information on the ray that feeds the discontinuity. For example, on the shock locus separating regions III and V, the C_- characteristic equation gives (see figure 6*b*)

$$u_m - 2c_m = u_b - 2c_b. \tag{4.5}$$

The values of u_b and c_b can then be determined from a Newton–Raphson iteration with c_b at the previous time as a starting condition. The values of u_f and c_f ahead of the shock in region III are given by

$$u_f = \tfrac{2}{3}(1 + x_{sn}/t_n), \quad c_f = \tfrac{1}{3}(2 - x_{sn}/t_n); \tag{4.6}$$

the shock velocity is then obtained from (2.9). Initially, we locate the bore at time t_n, using forward differences

$$x_{sn} = x_s + U(t_n - t),$$

where the shock velocity U is evaluated at time t. The new shock location is recomputed using central differences and the average of the shock velocities; the shock

conditions are recomputed as well. This process is repeated until the change in shock position is insignificantly small.

We adopted central differences for our computations because forward differences sometimes introduce numerical instabilities. Few individual computations required more than three or four iterations to converge to the central difference.

Results were relatively insensitive to the number of x-position nodes employed; we generally used 50–100. Time steps were interpolated as necessary to ensure that the plus- and minus-characteristics to interior nodes at the new time depended only on information at the previous time.

The shock eventually reaches the back of the tank at $x = -R/H$. The reflexion of the bore from the rear wall of the tank is determined from the shock conditions using the known values of c_f and u_f in region V and $u_b = 0$ at the wall. The locus is then computed, as before, until there is reflexion once again off the dyke. The process is continued in an entirely similar way for as long as desired.

For various values of L/H and R/H, computations were made to determine the percentage of original tank fluid which spilled over the dyke. This is

$$Q = \frac{H}{R}\int_0^T u_w(t)\, c_w^2(t)\, dt, \tag{4.7}$$

where u_w and c_w are values at the dyke. The shock locus was also calculated through several reflexions. Typical computer drawings of the water level c^2 between tank and dyke at various times are shown in figure 7. This sequence corresponds to the experimental situation shown in figure 2 and the individual plates are also set in corresponding positions. Qualitative agreement is evident; a more detailed comparison of computations with theory and experiment is given in § 6.

5. Experiments

Experiments were performed to complement (and to assess) the theory and also to explore quickly a number of modifications of the basic configuration. A Plexiglas tank was constructed which measured $9 \times 9 \times 48$ in. A removable wall 9 in. from one end divided the tank into a reservoir and a spillage channel. Dykes could be positioned along the channel as shown in figure 1; their impact surfaces had inclinations of 90°, 60° and 30°.

The reservoir was filled with water to a height H ($\leqslant 8$ in.) and the slide was subsequently removed as rapidly as possible. The surge was videotaped; slow motion playback was used to photograph the action and to measure the shock locus. Impact, overflow and shock formation for a vertical and a 60° inclined dyke are shown in figures 8 and 9 (plates 2 and 3). At the earliest times, before the effect of gravity is substantial, the flow at the vertical wall is similar to that described theoretically by Cumberbatch (1960). Some fluid is thrown high into the air as a plume which collapses into the main body of water that accumulates behind the shock and flows over the dyke.

The surge runs up the inclined dyke more easily and vaults a considerable distance behind it. Although there are significant dynamical differences in these cases, the spillages are commensurate. (Roughly, about 10 % more of the stored fluid spills over the inclined dyke.)

In order to measure the spillage due to the initial impact only, designated by Q_0, the slide was reinserted to prevent the reflected shock from returning to the dyke. (In all cases, the overflow had stopped when this action was taken.) If the shock were allowed to reverberate freely between wall and dyke, some additional spillage could occur on successive impacts. However, the total overflow, denoted by Q_1, was found to differ little from Q_0. For $L/R = 2$, the maximum difference is 5 %. (Sloshing is an important factor in the total spillage when L is small and a is large, i.e. for a high dyke very close to the wall of the tank.)

Measurements were made for various values of H, L and a (and the inclination angle). Each case was repeated at least three times and several hundred trials were made. The data were found to be reproducible with an average error of 2 %.

The height of the dyke for which the containment volume exactly equals the capacity of the storage tank is written as a_p. This is the height often prescribed by safety standards, which is the reason why it receives special attention.

6. Discussion

The principal finding concerning flow over a vertical dyke is that, within the parameter range studied, the volume fraction of fluid that escapes depends mainly on a/H, the ratio of the barrier height to that of the filled tank. Figure 10 indicates that the overflow or spillage fraction Q_0 is mainly a function of a/H for all combinations of barrier and tank heights in the range $\frac{1}{3} \leqslant L/R \leqslant 4$. The corresponding numerical calculations also show little dependence on L/R.

Figure 11 shows Q_0 *vs.* a_p/H (i.e. the containment and storage capacities are equal). Theory is in good agreement with observations; the larger values of Q_0 predicted are due in part to having neglected ground resistance and turbulence. The amount of fluid that escapes increases as the dyke is placed further from the wall and its height decreases accordingly to maintain the same volume capacity. (Of course, ground friction would ultimately negate this finding if extremely large values of L/H were involved, which is not the case in practice.) The measured spillage fraction Q_0 for each of three dykes of the same height but with inclinations of 30°, 60°, 90° is presented in figure 12. Obviously, a decrease in inclination from 90° allows more liquid to escape because the surging fluid retains much of its forward horizontal momentum during and after impact. As a result, the water vaults over the barrier and lands a considerable distance away. The spillage over an inclined dyke is at most twice that over a vertical wall of the same height. However, for most values of a/H, the differences are much smaller.

Although there is no explicit vertical velocity in the shallow-water theory, the law of conservation of mass enables the theory to account for the actual rise of fluid after it hits the wall. The height attained by the main body of fluid that accumulates behind the developing shock indicated by arrows in figure 13 (plate 4) is slightly larger than H, the original fluid level. The measured values exceed theoretical predictions by about 15 %.

The model cannot describe the flight of particles from the leading edge of the surge, which reach a height three times that of the tank. The amount of fluid involved is small although the collapsing plume does affect the movement of the shock.

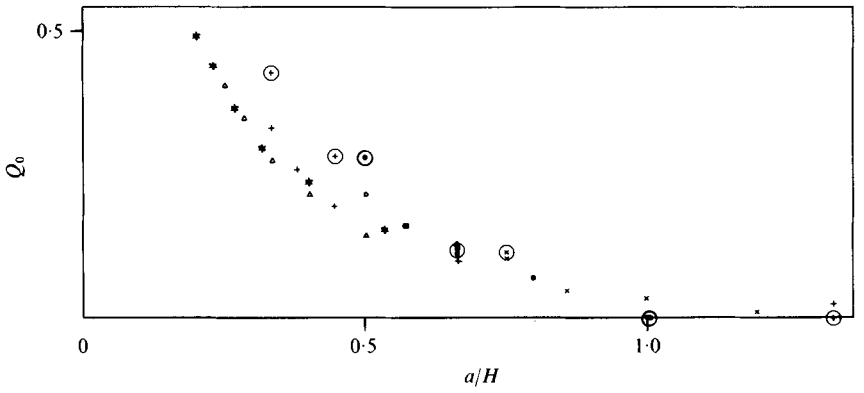

FIGURE 10. Spillage fraction *vs.* the ratio of the height of the dyke to that of the tank with L/R as a parameter. ×, $\frac{1}{2}$; ○, 1; +, 2; △, 3; *, 4. Circled points are numerically computed values.

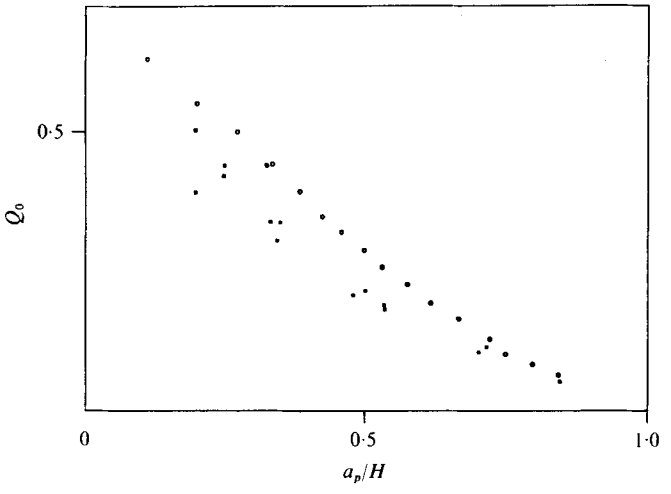

FIGURE 11. Spillage fraction *vs.* ratio of prescribed dyke height to tank height. ○, numerical calculation; □, experimental data.

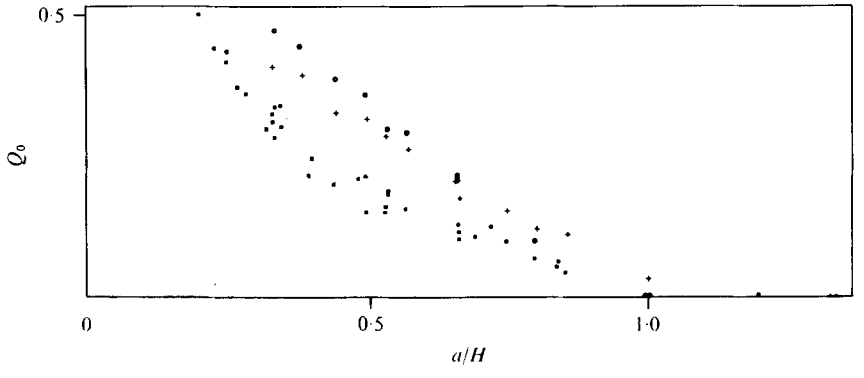

FIGURE 12. Spillage fraction as a function of a/H with the inclination angle of the dyke as a parameter. ○, 30°; +, 60°; ■, 90°.

Experimental and theoretical values of shock velocity are in good agreement but a consistent spatial displacement exists regarding the actual position of the bore. Part of this discrepancy is due to the fact that the real fluid hits the dyke somewhat later than predicted because friction and ground resistance slow the surge. Presumably, the results could be improved by including these effects in the model (Whitham 1955). (Our data on the arrival time of the front at the dyke agree with results of Dressler 1954.) However, there is also some difficulty in discerning and measuring the position of the shock just after impact. The shallow-water equations are perhaps most limited in describing events during this short period of intense vertical motion, although the theory predicts the main features of both flow and spillage remarkably well.

The overflow boundary condition (2.7), which is based in the local critical wave speed, seems generally satisfactory. Spillage must depend to an extent on the shape of the back of the dyke (where the water leaves the solid surface) as well as motion on top of the wall but a more refined theory would be required to treat these (secondary?) effects.

In circular geometries, the rushing liquid spreads as it flows from the ruptured wall to the dyke. Although this sideways motion must decrease the spillage, exploratory experiments indicate that the volume lost is still of the same order of magnitude as that calculated for the unidirectional flows examined here. It is anticipated that up to 25 % of the stored fluid could escape from the containment area by surmounting a barrier of prescribed height a_p. A sloping dyke permits an even larger amount of spillage since the fluid vaults the dyke in addition to simply spilling over owing to accumulation.

The comparison of theory and experiment for the same simple geometry establishes the relevance and accuracy of the model and of the specific approximations made. All of this is a necessary prelude to the creation of computer simulations of surges within actual installations or to design studies, when experiments are not feasible. The numerical and theoretical techniques developed in this study may be useful in these endeavours.

This research was partially supported by the United States Air Force Grant no. 77–3234 and The United States General Accounting Office. Miss E. Greenspan served as laboratory assistant.

REFERENCES

CUMBERBATCH, E. 1960 *J. Fluid Mech.* **7**, 353.

DRESSLER, R. F. 1954 *Int. Assoc. Hyd. Assemblée Générale de Rome*, vol. III, p. 319.

WHITHAM, G. B. 1955 *Proc. Roy. Soc.* A **227**, 339.

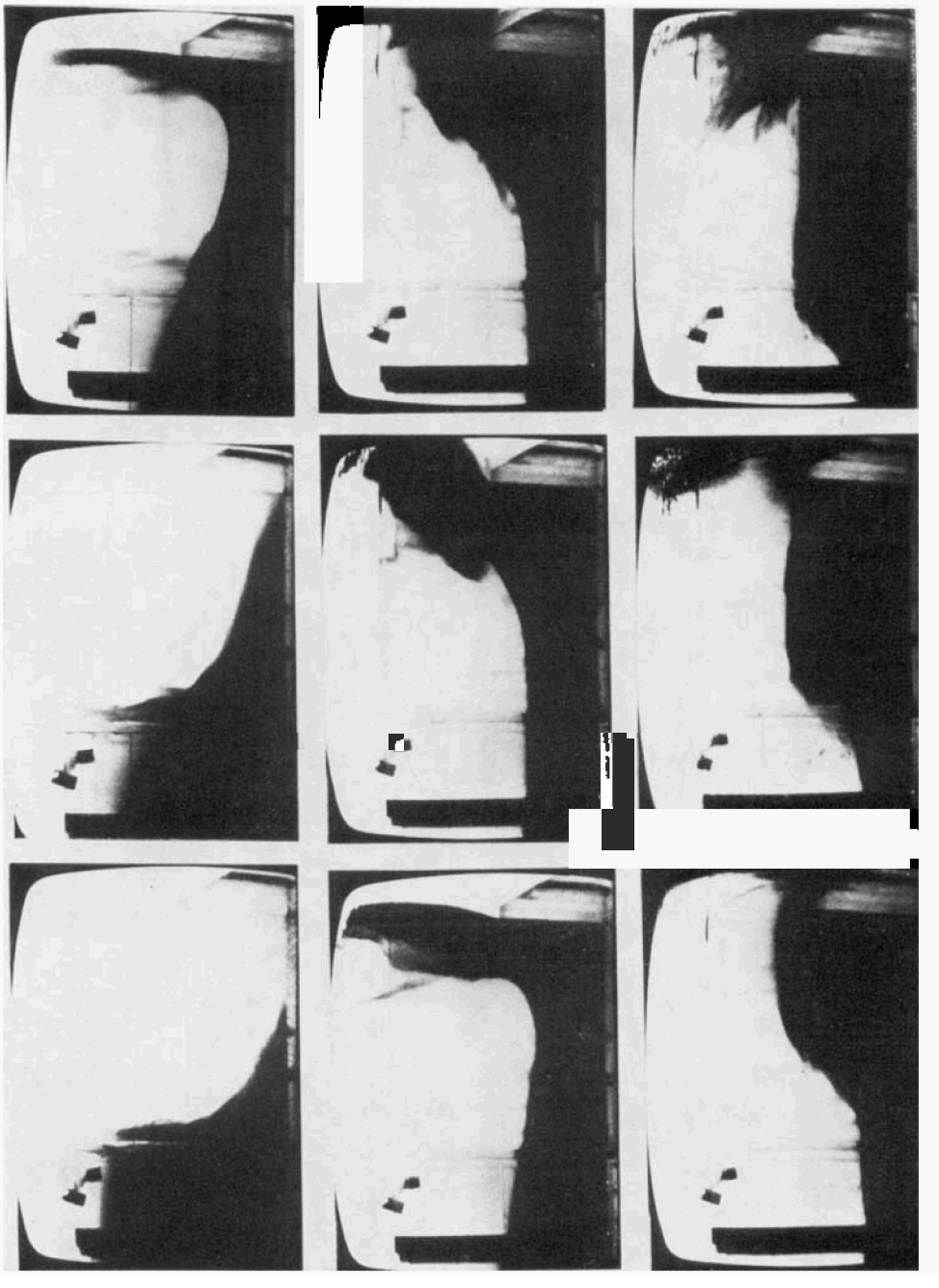

FIGURE 2. Collapse and surge against a dyke showing overflow and the formation of a shock. The photos are taken approximately 0·1 s apart. In the notation of figure 1, $H = 8$ in., $R = 9$ in., $L = 9$ in., $a = 4$ in.

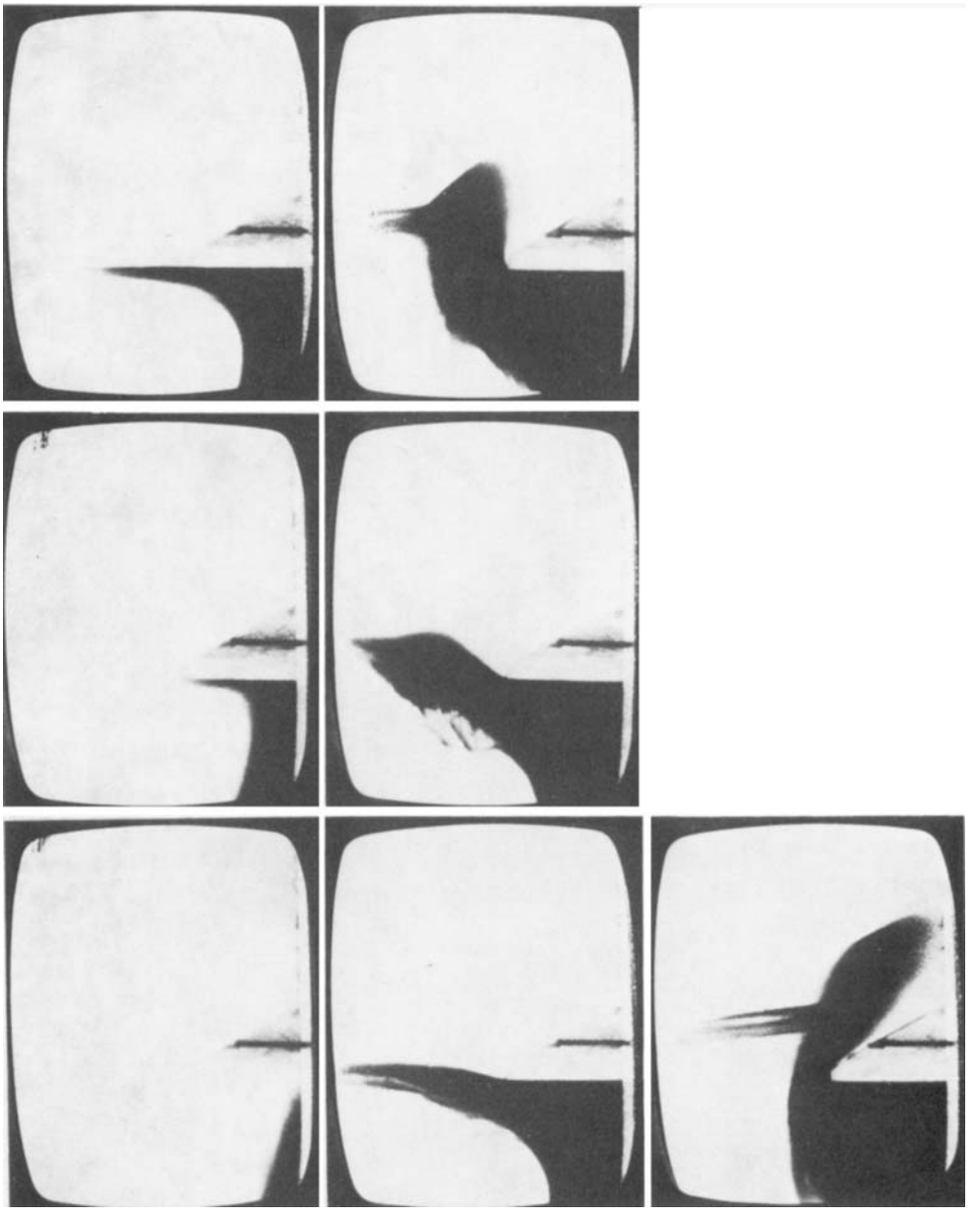

FIGURE 8. Flow over a vertical dyke when $H = 8$ in., $R = 9$ in., $L = 9$ in. and $a = 4$ in. (Containment volume equals storage volume.) Photo sequence corresponds, approximately, to 0·07 s intervals.

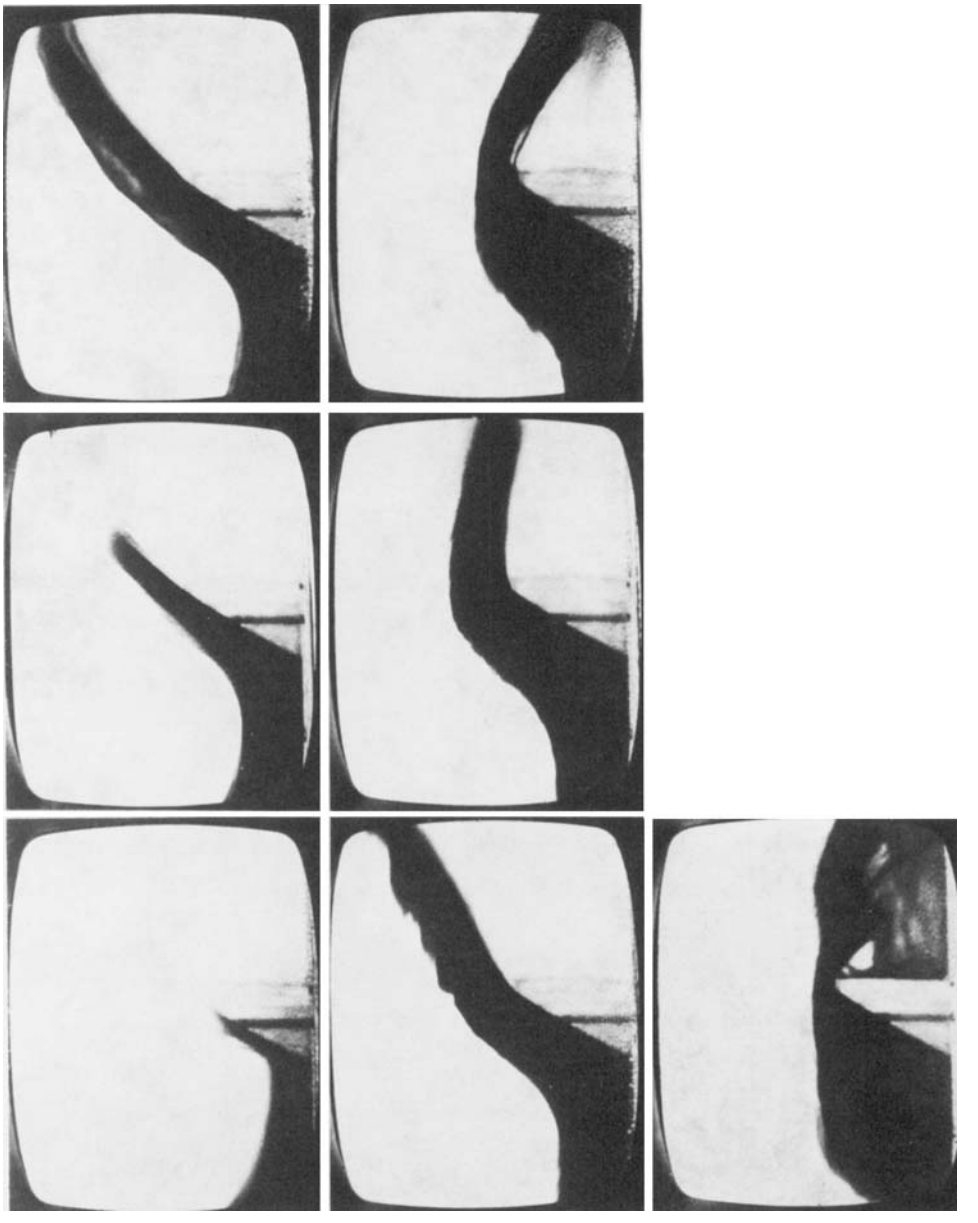

FIGURE 9. Flow over a 60° inclined dyke when $H = 8$ in., $R = 9$ in., $L = 9$ in. and $a = 4$ in. (Containment volume equals storage volume.) Photo sequence corresponds, approximately, to 0·1s intervals.

FIGURE 13. Impact sequence showing the overflow and formation of a shock. Theory accounts well for fluid motion below the height indicated by the arrows. Particles in the liquid jet above this are essentially in free flight and reach a height about three times that of the tank.